Effect of welding speed on microstructures and mechanical properties of underwater friction stir welded 2219 aluminum alloy

ARTICLE *in* MATERIALS AND DESIGN · MARCH 2011

Impact Factor: 3.5 · DOI: 10.1016/j.matdes.2010.09.032

Materials and Design 32 (2011) 1548–1553

Contents lists available at ScienceDirect

Materials and Design

journal homepage: www.elsevier.com/locate/matdes

Short Communication

Effect of welding speed on microstructures and mechanical properties of underwater friction stir welded 2219 aluminum alloy

H.J. Liu *, H.J. Zhang, L. Yu

State Key Laboratory of Advanced Welding Production Technology, Harbin Institute of Technology, Harbin 150001, PR China

ARTICLE INFO

Article history:
Received 20 July 2010
Accepted 27 September 2010
Available online 1 October 2010

ABSTRACT

Underwater friction stir welding (underwater FSW) has been demonstrated to be available for the strength improvement of normal FSW joints. In the present study, a 2219 aluminum alloy was underwater friction stir welded at a fixed rotation speed of 800 rpm and various welding speeds ranging from 50 to 200 mm/min in order to clarify the effect of welding speed on the performance of underwater friction stir welded joint. The results revealed that the precipitate deterioration in the thermal mechanically affected zone and the heat affected zone is weakened with the increase of welding speed, leading to a narrowing of softening region and an increase in lowest hardness value. Tensile strength firstly increases with the welding speed but dramatically decreases at the welding speed of 200 mm/min owing to the occurrence of groove defect. During tensile test, the joint welded at a lower welding speed is fractured in the heat affected zone on the retreating side. While at higher welding speed, the defect-free joint is fractured in the thermal mechanically affected zone on the advancing side.

1. Introduction

Friction stir welding (FSW) has been widely utilized to weld heat treatable aluminum alloys that were difficult to fusion weld. However, a soften region composed of the weld nugget zone (WNZ), the thermal mechanically affected zone (TMAZ) and the heat affected zone (HAZ) tends to be created due to the deterioration (coarsening or dissolution) of strengthening precipitates caused by FSW thermal cycles [1–4]. As a consequence, the tensile strength of the joint is lower than that of the base metal. In order to improve the joint performances by controlling the temperature level, external liquid cooling has been applied during FSW by several researchers. Benavides et al. [5] developed FSW experiment of 2024 Al using liquid nitrogen cooling to decrease the starting temperature of plates to be welded from 30 °C to −30 °C. The hardness in the TMAZ and HAZ was improved compared to the normal joint, but void defect was formed in the nugget and the cooling effect on mechanical properties of the joints was not stated in detail. Fratini et al. [6] considered in-process heat treatment with water flowing on the top surface of the samples during FSW. The tensile strength of the joint was found to be improved by the cooling action. In order to take full advantage of the heat absorption effect of water, underwater friction stir welding (underwater FSW) was proposed and conducted by the present authors [7]. The results indicated that the tensile strength of the underwater joint was significantly higher than that of the normal joint, confirming the feasibility of underwater FSW to improve the mechanical properties of the normal joints. Although external water cooling has been demonstrated to be available for the strength improvement in the previous studies, the relationship between the process variables and the performance of the cooled joint has not yet been developed. Therefore, a 2219 aluminum alloy was underwater friction stir welded in the present study, and the effect of welding speed on joint quality was investigated in terms of microstructures, hardness distributions and tensile properties.

2. Experimental procedure

The base metal (BM) utilized in the experiment was a 2219-T6 aluminum alloy plate with the thickness of 7.5 mm. The chemical compositions and mechanical properties of the BM are listed in Table 1. The plate was machined into rectangular welding samples with dimension of 300 mm long by 100 mm wide. After cleaned by acetone, the samples were clamped to the backing plate in a vessel, and then the water at room temperature was poured into the vessel to immerse the top surface of the samples. Underwater FSW was performed using an FSW machine (FSW-3LM-003) along the longitudinal direction (perpendicular to the rolling direction) at a fixed rotation speed and various welding speeds. The conical welding tool size and welding parameters are listed in Table 2.

After welding, the joints were all cross-sectioned perpendicular to the welding direction for metallographic analyses and Vicker's hardness tests using an electrical-discharge cutting machine. The cross-sections of the metallographic specimens were polished using a diamond paste, etched with Keller's reagent and observed

* Corresponding author. Tel.: +86 451 8641 3951; fax: +86 451 8641 6186.
E-mail address: liuhj@hit.edu.cn (H.J. Liu).

0261-3069/$ - see front matter © 2010 Elsevier Ltd. All rights reserved.
doi:10.1016/j.matdes.2010.09.032

Table 1
Chemical compositions and mechanical properties of 2219 aluminum alloy.

Chemical compositions (wt.%)									Mechanical properties	
Al	Cu	Mn	Fe	Ti	V	Zn	Si	Zr	Tensile strength	Elongation
Bal.	6.48	0.32	0.23	0.06	0.08	0.04	0.49	0.20	432 MPa	11%

Table 2
Tool size and welding parameters used in the experiments.

Tool size (mm)			Welding parameters			
Shoulder diameter	Pin diameter	Pin length	Rotation speed (rpm)	Welding speed (mm/min)	Axial load (kN)	Tool tilt (°)
22.5	7.5	7.4	800	50–200	4.6	2.5

by an optical microscopy (OM, Olympus-MPG3). The corresponding microstructures to WNZ, TMAZ, HAZ and BM were extracted from Regions A–E at the weld midplane, as marked in Fig. 1, where RS and AS represent the retreating side and the advancing side, respectively. Region A was located in the weld nugget center, Regions B and C were the TMAZ adjacent to the WNZ on both sides of the weld, Region D was the HAZ adjacent to the TMAZ, and Region E was the BM far from the weld center. Microhardness profiles were measured at the mid-thickness of the polished cross-sections with a spacing of 1 mm between the adjacent indentations. The testing load was 4.9 N for 10 s.

Transmission electron microscopy (TEM PHILIPS CM12) was used to determine the precipitate distribution. The foil disk specimens for TEM were cut parallel to the welding direction from the TMAZ (Region C), the HAZ (Region D) and the BM (Region E). The electron transparent thin sections were prepared through double jet electro-polishing using a solution of 30% nitric acid in methanol (18 V and −35 °C).

The transverse tensile specimens were prepared with reference to China National Standard GB/T2651-2008 (equivalent to ASTM B557-02). The room temperature tensile test was performed at a crosshead speed of 1 mm/min using a computer-controlled testing machine (Instron-1186). The tensile properties of each joint were evaluated using three tensile specimens cut from the same joint. After tensile test, the fracture features of the joints were analysed by the OM mentioned above.

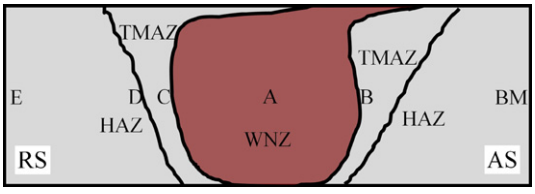

Fig. 1. The schematic view of exact locations where microstructural analyses are performed.

3. Results and discussion

3.1. Macro and microstructures of the joints

Fig. 2 shows the macroscopic appearances of the joints welded at different welding speeds. No welding defects can be observed in the joints produced at the welding speed of 50–150 mm/min, whereas the groove defect is formed on the AS at the welding speed of 200 mm/min. The nugget size decreases with increasing the welding speed, which is attributed to the lowering of material flow level around the tool pin.

The WNZ is characterized by fine equiaxed grains due to the dynamic recrystallization during FSW (Fig. 3). The grain size varies significantly with the welding speed. As the welding speed increases from 50 to 200 mm/min, the average size of the refined grains is determined to 6.8 μm, 7.5 μm, 10 μm and 2.5 μm respectively by the mean-linear-intercept method. That is to say, the grain size firstly increases from 50 to 150 mm/min and then decreases to a rather low value at 200 mm/min. This evolving trend of grain size with the welding speed may be resulted from the synergetic effects of material deformation and heat input during FSW. The increase of welding speed results in a decrease in both the degree of material deformation and the heat input during FSW. The decrease in degree of material deformation generally leads to an increase in the recrystallized grain size [8–11], while the decrease in heat input tends to result in a grain refinement. Therefore the variation of grain size with welding speed depends on which factor is dominant. It seems that the material deformation mainly controls the grain size at welding speed lower than 150 mm/min. At relatively high welding speed of 200 mm/min, it is the heat input that dominants the final grain size.

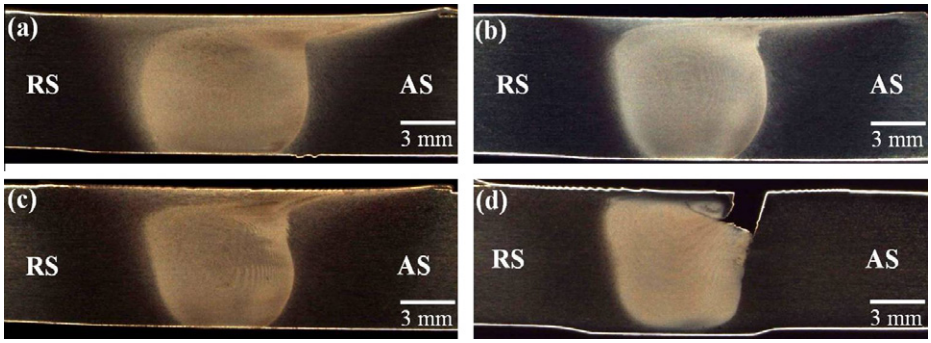

Fig. 2. Cross sections of the joints welded at different welding speeds: (a) 50 mm/min, (b) 100 mm/min, (c) 150 mm/min and (d) 200 mm/min.

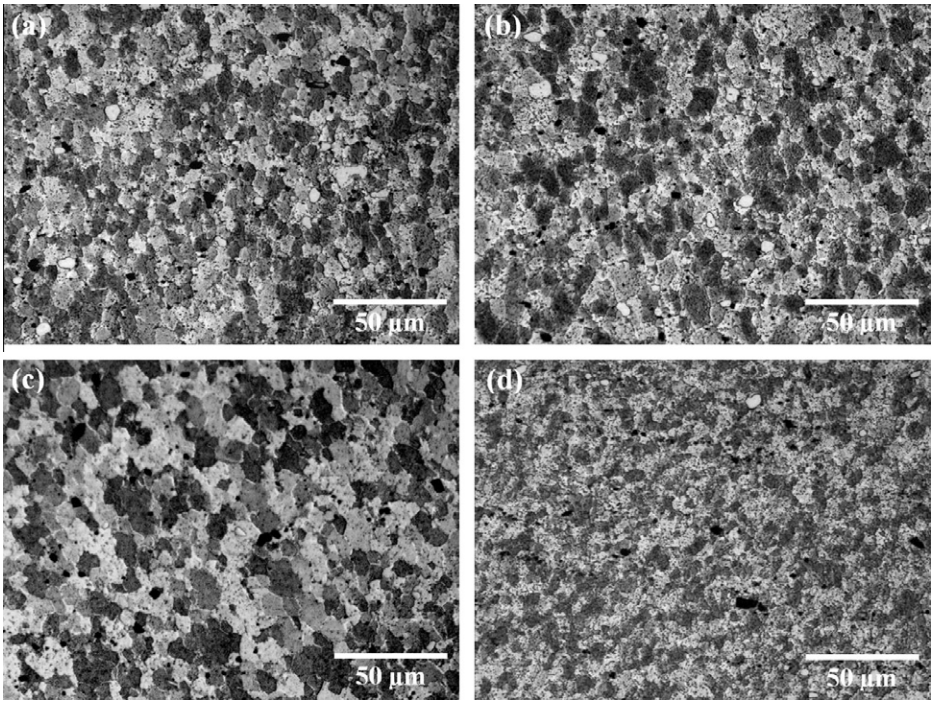

Fig. 3. Grained structures of the WNZ formed at different welding speeds: (a) 50 mm/min, (b) 100 mm/min, (c) 150 mm/min and (d) 200 mm/min.

In the TMAZ and the HAZ, little variations in grained structures can be observed with the increase of welding speed. The representative grained structures of the TMAZ and the HAZ are shown in Fig. 4. The grains are highly extruded and elongated in the TMAZ on the AS (Fig. 4a), which creates a sharper interface between the WNZ and the TMAZ. This is in contrast with the RS of the weld, where the WNZ/TMAZ interface is rather unclear (Fig. 4b). The HAZ only experiences welding thermal cycles and no plastic deformation occurs in this region during FSW, hence the HAZ displays similar grained structures with the BM (see Fig. 4c and d).

However, the precipitate evolution is notable in the TMAZ and the HAZ as the welding speed increases. Fig. 5a–e shows the precipitates lying on {1 0 0} planes of the matrix in the BM, HAZ and TMAZ of the joints. The plate-like precipitates densely distributed in the BM, 54 nm in diameter and 4 nm in thickness, are believed to be meta-stable θ' phases according to the previous studies [12–14]. The θ' precipitates can be coarsened, transformed to stable state or dissolved into the matrix during FSW with increasing the temperature level.

At lower welding speed of 50 mm/min, the θ' precipitates in the HAZ exhibit a significant coarsening and a dramatical decrease in

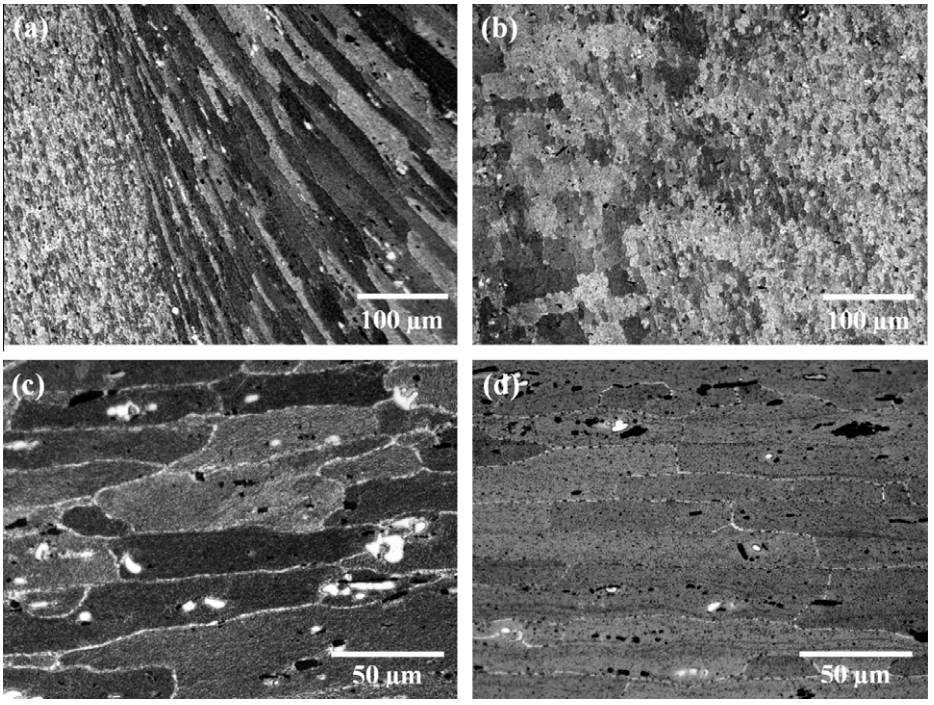

Fig. 4. Representative grained structures of the TMAZ, the HAZ and the BM (obtained at 150 mm/min): (a) TMAZ on the AS, (b) TMAZ on the RS, (c) HAZ and (d) BM.

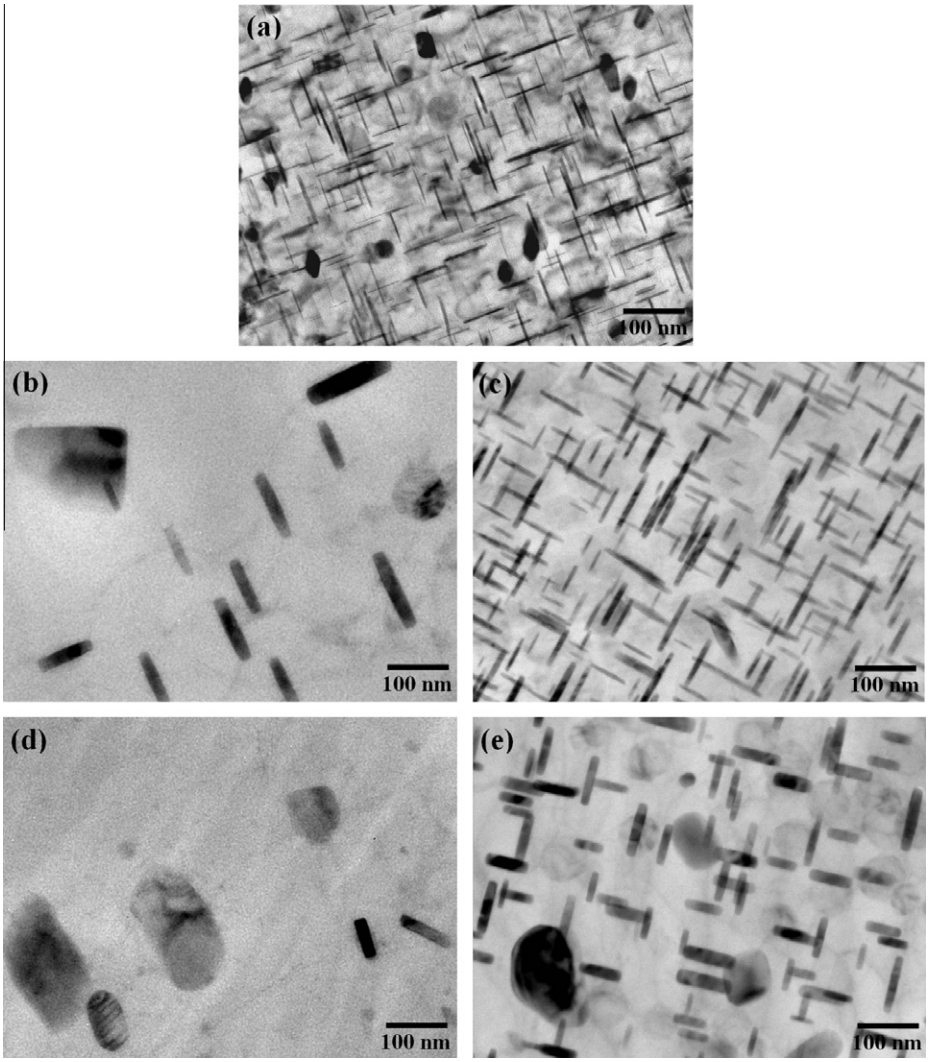

Fig. 5. The precipitates distributed in different zones of the joints welded at different welding speeds: (a) BM, (b) HAZ formed at 50 mm/min, (c) HAZ formed at 150 mm/min, (d) TMAZ formed at 50 mm/min and (e) TMAZ formed at 150 mm/min.

density (Fig. 5b). The size of the precipitates is 114 nm in diameter and 25 nm in thickness, much larger than that of the BM. In the TMAZ, the θ' precipitates nearly disappear and have been transformed to the block-shaped equilibrium θ precipitates (Fig. 5d). The considerably low density compared to the BM implies that precipitate dissolution should also occur in the region. However, when the welding speed increases (e.g. 150 mm/min), the precipitate evolution exhibits quite different features. In the HAZ, the size of the θ' precipitates only reaches 70 nm in diameter and 7 nm in thickness (Fig. 5c), and the precipitate density is also higher than that obtained at 50 mm/min, suggesting a remarkable lowering in precipitate coarsening level. On the other hand, a large quantity of θ' precipitates having a diameter of 90 nm and a thickness of 18 nm are still distributed in the TMAZ (Fig. 5e), indicating that the precipitate deterioration in the TMAZ is also retarded by increasing the welding speed.

3.2. Microhardness distributions of the joints

Microhardness distributions on the transverse cross-section of the joints are shown in Fig. 6. The hardness of the BM is in the range of 120–130 Hv. A softening region having lower hardness value than the BM exist in all the joints welded at different welding speeds. The hardness of the TMAZ and the HAZ increases with increasing the welding speed, leading to a gradual narrowing of the softening region. This is attributed to the weakening of precipitate deterioration in the two regions as the welding speed

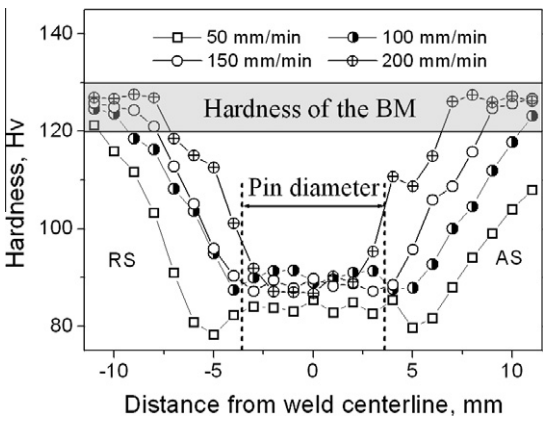

Fig. 6. Microhardness distributions of the joints welded at different welding speeds.

increases (Fig. 5). The lowest hardness of the joint welded at 50 mm/min is located in the HAZ adjacent to the TMAZ on the RS. When the welding speed increases to 100 and 150 mm/min, the lowest hardness is at the TMAZ adjacent to the WNZ on either side of the weld. For the joint welded at 200 mm/min, the lowest hardness is lying in the WNZ. That means the lowest hardness region of the joint moves towards the weld center with increasing the welding speed. Furthermore, the lowest hardness value increases with the welding speed, resultant from the lowering of precipitate deterioration level at the weakest location of the joint (see Fig. 5b and e).

In the joint welded at 50 mm/min, the TMAZ appears to have experienced larger extent of precipitate deterioration than the HAZ (see Fig. 5b and d), but the lowest hardness region is lying in the HAZ rather than the TMAZ. This may be attributed to the large quantity of dissolved precipitates in the TMAZ which can increase the concentration of solute atoms available for the solid solution strengthening and even precipitation hardening during natural aging. As a result, the TMAZ exhibits higher hardness value than the HAZ.

3.3. Tensile properties of the joints

Fig. 7 shows the tensile properties of the joints as a function of welding speed. The tensile strength firstly increases with increasing the welding speed from 50 to 150 mm/min and then dramatically decreases to a considerably low level owing to the formation of groove defect. The maximum tensile strength is found to be 347 MPa, equivalent to 80% of that of the BM. The joint ductility seems to follow the similar behavior to the tensile strength, and the maximum elongation, 8.8%, is achieved at the welding speed of 150 mm/min, equivalent to 80% of that of the BM.

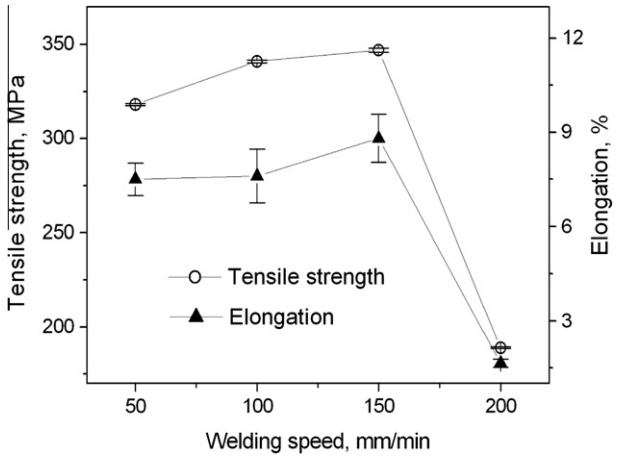

Fig. 7. Tensile properties of the joints welded at different welding speeds. Error bars are based on the standard deviation.

The fracture features vary significantly with the welding speed for the defect-free joints, as seen from Fig. 8. At lower welding speed of 50 mm/min, the tensile specimens of the joint are all fractured in the HAZ adjacent to the TMAZ on the RS (Fig. 8a), consistent with the lowest hardness region of the joint (see Fig. 6). When the welding speed increases to 100 and 150 mm/min, the tensile specimens of the both joints are all fractured in the TMAZ adjacent to the WNZ on the AS (Fig. 8b and c), also corresponding to their separate weakest locations. Notably the fracture occurs in the TMAZ on the AS rather than on the RS in these two cases although the lowest hardness is located on both sides of the weld. The reason for this is that a sharper WNZ/TMAZ interface exists on the AS in contrast to the RS (see Fig. 4a and b). During tensile test, the sharper interface causes a mismatch material deformation in the WNZ and the TMAZ, thus the microcracking tends to be firstly formed in the weakest location adjacent to the interface. Since fracture tends to occur in the lowest hardness region, the increase of lowest hardness value is in nature responsible for the strength improvement when the welding speed increases from 50 to 150 mm/min.

In a word, the welding speed must be chosen in a proper range in order to obtain high-quality joint through underwater FSW. The lower welding speed (e.g. 50 mm/min) can increase the heat input into the welding samples, leading to dramatical precipitate deterioration. The joint is fractured in the HAZ during tensile test and presents relative low tensile properties. As the welding speed increases, the coarsening and transformation of the θ' precipitates are weakened due to the lowering of heat input. Consequently, the softening region is narrowed and the weakest location is shifted to the TMAZ adjacent to the WNZ with lesser strength loss during tensile test. If the welding speed increases to a rather high value (e.g. 200 mm/min), groove defect can be formed which significantly deteriorates the joint properties.

4. Conclusions

A 2219 aluminum alloy has been underwater friction stir welded and the effect of welding speed on microstructures and mechanical properties of the joints was investigated in detail. The conclusions of significance are drawn as follows:

(1) The grain size in the WNZ gradually increases with the increase of welding speed from 50 to 150 mm/min but abruptly decreases at 200 mm/min. This should be attributed to the variation of the dominant factors governing the grain size before and after 150 mm/min.

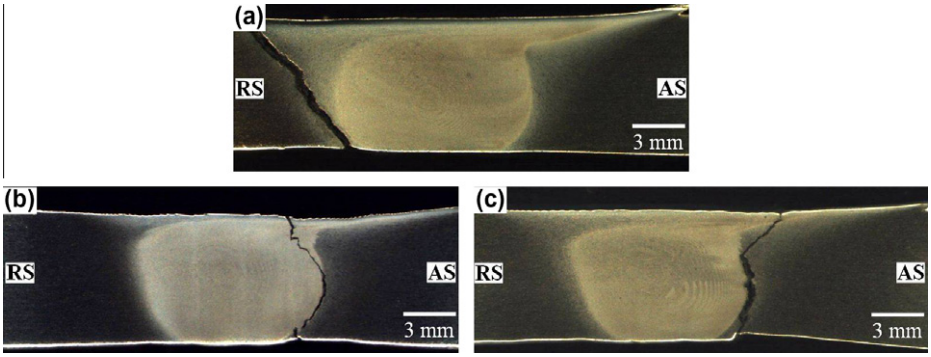

Fig. 8. Fracture locations of the joints welded at different welding speeds: (a) 50 mm/min, (b) 100 mm/min and (c) 150 mm/min.

(2) The precipitate deterioration in the TMAZ and HAZ becomes weaker by increasing the welding speed, causing a narrowing of the softening region and an increase of the lowest hardness value.
(3) The tensile strength of the defect-free joints increases with increasing the welding speed. The maximum tensile strength is 347 MPa, equivalent to 80% of that of the BM.
(4) The fracture features of the joints are largely dependent on the welding speed. At low welding speed of 50 mm/min, the joint is fractured in the HAZ adjacent to the TMAZ on the RS. When the welding speed increases to 100 and 150 mm/min, fracture tends to occur at the TMAZ adjacent to the WNZ on the AS.

Acknowledgements

The authors are grateful to be supported by the National Basic Research Program of China (973 Program, 2010CB731704) and by the National Science and Technology Major Project of China (302010ZX04007-011).

Reference

[1] Fonda RW, Bingert JF. Microstructural evolution in the heat-affected zone of a friction stir weld. Metall Mater Trans A 2004;35:1487–99.
[2] Mishra RS, Ma ZY. Friction stir welding and processing. Mater Sci Eng R 2005;50:1–78.
[3] Simar A, Bréchet Y, Meester B-De, Denquin A, Pardoen T. Microstructure, local and global mechanical properties of friction stir welds in aluminium alloy 6005A-T6. Mater Sci Eng A 2008;486:85–95.
[4] Starink MJ, Seschamps A, Wang SC. The strength of friction stir welded and friction stir processed aluminum alloys. Scripta Mater 2008;58:377–82.
[5] Benavides S, Li Y, Murr LE, Brown D, McClure JC. Low-temperature friction-stir welding of 2024 aluminum. Scripta Mater 1999;41:809–15.
[6] Fratini L, Buffa G, Shivpuri R. In-process heat treatments to improve FS-welded butt joints. Int J Mach Tool Manufact 2009;43:664–70.
[7] Liu HJ, Zhang HJ, Huang YX, Yu L. Mechanical properties of underwater friction stir welded 2219 aluminum alloy. Trans Nonferrous Met Soc China 2010;20:1387–91.
[8] Jata KV, Semiatin SL. Continuous dynamic recrystallization during friction stir welding of high strength aluminum alloys. Scripta Mater 2000;43:743–9.
[9] Jazaeri H, Humphreys FJ. The transition from discontinuous to continuous recrystallization in some aluminum alloys I–the deformed state. Acta Mater 2004;52:3239–50.
[10] Prangnell PB, Heason CP. Grain structure formation during friction stir welding observed by the stop action technique. Acta Mater 2005;53:3179–92.
[11] Sakai T, Miura H, Yang X. Ultrafine grain formation in face centered cubic metals during severe plastic deformation. Mater Sci Eng A 2009;499:2–6.
[12] Chen YC, Feng JC, Liu HJ. Precipitate evolution in friction stir welding of 2219-T6 aluminum alloys. Mater Charact 2009;60:476–81.
[13] Srinivasan PB, Arora KS, Dietzel W, Pandey S, Schaper MK. Characterisation of microstructure, mechanical properties and corrosion behaviour of an AA2219 friction stir weldment. J Alloy Compd 2010;492:631–7.
[14] Paglia CS, Buchheit RG. Microstructure, microchemistry and environmental cracking susceptibility of friction stir welded 2219-T87. Mater Sci Eng A 2006;429:107–14.